

Uncharacterized bacterial structures revealed by electron cryotomography

Megan J. Dobro¹, Catherine M. Oikonomou², Aidan Piper¹, John Cohen¹, Kylie Guo², Taylor Jensen², Jahan Tadayon², Joseph Donermeyer², Yeram Park², Benjamin A. Solis³, Andreas Kjær⁴, Andrew I. Jewett², Alasdair W. McDowall², Songye Chen², Yi-Wei Chang², Jian Shi⁵, Poorna Subramanian², Cristina V. Iancu⁶, Zhuo Li⁷, Ariane Briegel⁸, Elitza I. Tocheva⁹, Martin Pilhofer¹⁰, Grant J. Jensen^{2,11,*}

¹ Hampshire College, 893 West St., Amherst, MA 01002

² California Institute of Technology, 1200 E. California Blvd., Pasadena, CA 91125

³ University at Albany, SUNY, 135 Western Avenue, Albany, NY. 12203

⁴ University of Southern Denmark, Campusvej 55, 5230 Odense M, Denmark

⁵ National University of Singapore, 21 Lower Kent Ridge Road, Singapore 119077

⁶ Rosalind Franklin University of Medicine and Science, 3333 Green Bay Rd., North Chicago, IL 60064

⁷ City of Hope, 1500 E. Duarte Road, Duarte, CA 91010

⁸ Leiden University, Sylvius Laboratories, Sylviusweg 72, 2333 BE, Leiden, Netherlands

⁹ University of Montreal, C.P. 6128, succursale Centre-ville, Montreal, Quebec, Canada

¹⁰ ETH Zurich, Otto-Stern-Weg 5, 8093 Zurich, Switzerland

¹¹ Howard Hughes Medical Institute, 1200 E. California Blvd., Pasadena, CA 91125

* To whom correspondence should be addressed. Tel: (626) 395-8827. Email:

jensen@caltech.edu

Running title: ECT of novel bacterial structures

Keywords: bacteria, electron cryotomography, cryo-EM, bacterial ultrastructure, uncharacterized structures

SUMMARY STATEMENT

Here we present a survey of previously uncharacterized structures we have observed in bacterial cells by electron cryotomography, in the hopes of spurring their identification and study.

ABSTRACT

Electron cryotomography (ECT) can reveal the native structure and arrangement of macromolecular complexes inside intact cells. This technique has greatly advanced our understanding of the ultrastructure of bacterial cells. Rather than undifferentiated bags of enzymes, we now view bacteria as structurally complex assemblies of macromolecular machines. To date, our group has applied ECT to nearly 90 different bacterial species, collecting more than 15,000 cryotomograms. In addition to known structures, we have observed several, to our knowledge, uncharacterized features in these tomograms. Some are completely novel structures; others expand the features or species range of known structure types. Here we present a survey of these uncharacterized bacterial structures in the hopes of accelerating their identification and study, and furthering our understanding of the structural complexity of bacterial cells.

INTRODUCTION

The history of cell biology has been punctuated by advances in imaging technology. In particular, the development of electron microscopy in the 1930s produced a wealth of new information about the ultrastructure of cells (Ruska, 1987). For the first time, the structure of cell envelopes, internal organelles, cytoskeletal filaments and even large macromolecular complexes like ribosomes became visible. A further advance came in the 1980s and 1990s with the development of electron cryotomography (ECT) (Koster *et al.*, 1997), which allows small cells to be imaged intact in 3D in a near-native, “frozen-hydrated” state to “macromolecular” (~4 nm) resolution, without the limitations and artifacts of more traditional specimen preparation methods (Pilhofer *et al.*, 2010).

ECT has helped reveal the previously unappreciated complexity of “simple” bacterial cells. Our group has been using ECT to study bacteria for more than a decade, generating more than 15,000 tomograms of 88 different species. These tomograms have revealed new insights into, among other things, the bacterial cytoskeleton (Komeili *et al.*, 2006, Li *et al.*, 2007, Pilhofer *et al.*, 2011, Swulius & Jensen, 2012), cell wall architecture (Gan *et al.*, 2008, Beeby *et al.*, 2013), morphogenesis (Ebersbach *et al.*, 2008), metabolism (Iancu *et al.*, 2007), motility (Murphy *et al.*, 2006, Chen *et al.*, 2011, Abrusci *et al.*, 2013, Chang *et al.*, 2016), chemotaxis (Briegleb *et al.*, 2012), sporulation (Tocheva *et al.*, 2011), cell-cell interactions (Basler *et al.*, 2012), and phage infection (Guerrero-Ferreira *et al.*, 2011) (for a summary with more references from our and others’ work, see (Oikonomou & Jensen, 2016)).

A major hurdle in such studies is identifying the novel structures observed in tomograms. In some cases, we have identified structures by perturbing the abundance (either by knockout or overexpression) of candidate proteins (Ingerson-Mahar *et al.*, 2010). In others, we have used correlated light and electron microscopy (CLEM) to locate tagged proteins of interest (Briegel *et al.*, 2008, Chang *et al.*, 2014). In one striking example, we observed 12- and 15-nm tubes in our tomograms of *Vibrio cholerae* cells. Ultimately, in collaboration with John Mekalanos' group, we identified them as type VI secretion systems (T6SS), which immediately led to the insight that the bacterial T6SS functions as a phage-tail-like, contractile molecular dagger (Basler *et al.*, 2012).

Many other novel structures we have observed, though, remain unidentified. In some cases, we have published papers describing the novel structures seen in a particular species (e.g. (Murphy *et al.*, 2008, Muller *et al.*, 2014)), but many have never been published. We therefore conducted a visual survey of the tomograms collected by our group, curated in the Caltech Tomography Database (Ding *et al.*, 2015), as of 2015 and present here a catalog of previously undescribed bacterial structures. Some structures are, to our knowledge, completely novel; others belong to known types but present additional features or an expanded species range. We hope that sharing these images will help spur their identification and study, contributing to our expanding understanding of bacterial cell biology. In addition, we look forward to a future in which custom microbes are designed for diverse medical and industrial purposes; an expanded "parts list" of structures to be repurposed will aid in this effort.

RESULTS AND DISCUSSION

We performed a visual inspection of approximately 15,000 tomograms of intact, frozen-hydrated cells belonging to 88 species and identified what we believed to be novel structures. A summary of the results of this survey is shown in Supplementary Table 1, with features observed, species range, and frequency listed for each structure type. For full tomographic (3D) views of each feature, please see the accompanying supplementary movies at the following link: <https://figshare.com/s/782461843c3150d27cfa>.

Extracellular structures

External appendages

In several tomograms of *Prostheobacter debontii* we observed novel extracellular appendages, apparently attached to the cell membrane. Individual cells displayed up to 30 such appendages, which exhibited consistent size (~20 nm wide and ~50 nm long) and shape (Figure 1A). Subtomogram averaging of 105 particles revealed a distinctive structure: extending outward from the cell membrane, five legs were attached to a disc, which in turn connected to a smaller disc and a long neck region (Figure 1B,C). Individual particles showed that the structure culminated in two antenna-like filaments, which were likely averaged out in the average due to conformational variability. The appendages were observed in multiple cultures of the strain. While it remains unclear whether they originated intra- or extracellularly, no free-floating appendages were ever observed in the extracellular space. They may represent novel bacterial attachment organelles, a novel secretion system (though we would expect a cell envelope spanning complex) or a novel bacteriophage (though there is a notable lack of a capsid-like density).

We observed a different novel extracellular appendage in tomograms of *Azospirillum brasilense* cell poles. Thin hooks were seen extending out from the cell surface (Figure 2). Individual cells exhibited dozens of hooks, each ~3 nm wide and ~75 nm long, associated with the outer membrane. Hooks were seen in > 90% of wild-type cells as well as in a strain in which the operon encoding the Che1 chemotaxis system was deleted. They were seen in ~50 % of cells in which the Che4 chemotaxis system operon was deleted, and none were seen in cells lacking both the Che1 and Che4 operons. *A. brasilense* is a well-studied plant growth-promoting bacterium. Cells attach to plant roots through a two-step process (De Troch & Vanderleyden, 1996): a rapid, reversible adsorption thought to be mediated by the polar flagellum; and a slow, irreversible anchoring, thought to be mediated by an as-yet unidentified surface polysaccharide (Steenhoudt & Vanderleyden, 2000). A recent study reported that mutants in components of the Che4 chemotaxis system are defective in this root colonization (Mukherjee *et al.*, 2016). *A. brasilense* cells also attach to conspecifics in the presence of elevated oxygen levels (Bible *et al.*, 2015). Interestingly, it has been shown that mutants in components of the Che1 chemotaxis system form such attachments more rapidly than wild-type cells (Bible *et al.*, 2012). The hooks we observed are vaguely reminiscent of the grappling hook-like structures that an archaeal species uses to anchor itself in biofilms (Moissl *et al.*, 2005). It is therefore tempting to speculate that these hooks similarly play a role in adhesion, either to other *A. brasilense* cells or to plant roots.

In cells of strain JT5 (a bacterium isolated from termite gut and related to the *Dysgonomonas* genus), we observed abundant fimbriae concentrated at the cell poles (Figure 3). They were present in cells grown on cellulose or xylan, as well as in a condition inducing starvation. Their

width (~4 nm), apparent flexibility, density on the cell envelope, and inhomogeneous distribution around the cell is consistent with curli, functional amyloids secreted by the type VIII secretion system that are involved in adhesion (Epstein *et al.*, 2009, Van Gerven *et al.*, 2015). Curli systems are relatively divergent at the sequence level, but are remarkably widespread phylogenetically, and the genes were reported to be present in Bacteroidetes (the phylum containing *Dysgonomonas*) (Dueholm *et al.*, 2012). The appendages we observed in strain JT5 may therefore play a role in adhesion in the environment of the termite gut.

Outer membrane vesicle chains

A wide variety of Gram-negative Bacteria produce outer membrane vesicles (Kulp & Kuehn, 2010). Recently, chained or tubular outer membrane structures have also been identified in a few species. In *Delftia* sp. Cs1-4, tubular sheaths called “nanopods” deliver outer membrane vesicles some distance from the cell (Shetty *et al.*, 2011). In *Myxococcus xanthus*, chained extensions of the outer membrane transfer proteins and molecules between cells in a biofilm (Remis *et al.*, 2014). In *Shewanella oneidensis*, nanowires used for extracellular electron transport can take the form of outer membrane vesicle chains (Pirbadian *et al.*, 2014). We also observed chained extensions of the outer membrane in *Borrelia burgdorferi* strain B31 (Figure 4). Both spherical and tubular segments were observed in these chains. Outer membrane vesicles are important virulence factors in *B. burgdorferi* (Skare *et al.*, 1995), and lipid exchange was recently observed between *B. burgdorferi* and host cells (Crowley *et al.*, 2013); a chained vesicle morphology may aid in this process.

Intracellular structures

161 ***“Nanospheres”***

162 In three *Vibrio cholerae* cells (two from a C6706 lacZ⁻ strain (Cameron *et al.*, 2008), and one
163 from a Δ ctxA Δ tcpB strain (Chang *et al.*, 2016)) we observed clusters of “nanospheres” – hollow
164 granules with thick walls (Figure 5). The diameter of the nanospheres ranged from ~18-37 nm,
165 and the walls were ~4-10 nm thick. They were pleomorphic: most were roughly spherical, but
166 some were oblong or comma shaped. Each cluster contained about two dozen nanospheres. The
167 clusters were observed at the cell periphery, near the inner membrane (although the clusters were
168 large enough to extend to the center of the cell), and were always observed in close proximity to
169 a filament array structure (discussed below).

171 ***Filaments, bundles, arrays, chains and meshes***

172 One of the strengths of ECT imaging is its power to resolve cytoskeletal elements in small
173 bacterial cells. In addition to those we have already identified, we observed many novel
174 filamentous structures in tomograms, including filament arrays, bundles, chains and meshes
175 (Figure 6). In *Hyphomonas neptunium*, we observed long helical filament bundles in the
176 prosthecae that connect dividing cells (Figure 6A). The helix width was 9.5 ± 1.5 nm, the
177 spacing between cross-densities 6.0 ± 0.3 nm, and the helical pitch $\sim 26^\circ$. *H. neptunium* divides
178 by asymmetric budding (Weiner *et al.*, 2000) and the genome of the parent cell is passed to the
179 daughter cell through the narrow prostheca connecting the two cells (Zerfas *et al.*, 1997). We
180 observed that the helical structure was straightened in cells treated with ethidium bromide (an
181 intercalator known to unwind DNA (Pommier *et al.*, 1987)) (Figure 6B). We therefore propose
182 that the helix is composed of supercoiled DNA, with each visible filament a DNA duplex
183 connected to adjacent duplexes by cross-densities formed by an unidentified protein.

In *Helicobacter pylori* cells we observed extensive filament bundles. In one cell in an early stage of lysis, such bundles were observed throughout most of the cell (Figure 6C). In *V. cholerae* we observed filament arrays resembling a honeycombed mesh (Figure 6D). These arrays varied in length, but were usually fairly short (~100 nm in length and width), like the example shown in Figure 6E. This is the structure we observed near the nanosphere clusters. Filament arrays exhibited different morphologies in other species. *Thiomonas intermedia* cells contained untwisted arrays ~48 nm thick, ~30 nm wide (Figure 6F). In addition to the prosthecal helix described above, *H. neptunium* cells also contained a bundle of twisting filaments ladderred by cross-densities (Figure 6G). These bundles were ~40 nm thick and ~75 nm wide. In a *Hylemonella gracilis* cell we observed a helical bundle of filaments that varied in width and could be related to the nucleoid (Figure 6H). In *Halothiobacillus neapolitanus* c2 cells grown in limited CO₂ for several hours we observed linear filament arrays with prominent cross-densities spaced 7 ± 0.8 nm apart (Figure 6I). *Mycobacterium smegmatis* displayed straight arrays ~80 nm thick and wide, comprising segments of pitched filaments (Figure 6J). Filament arrays were also seen in multiple species of *Prostheco bacter*: *P. vanneervanii* contained linear chains (Figure 6K) and one *P. debontii* cell contained a straight array similar to those observed in *T. intermedia* (Figure 6L) as well as mesh-like arrays spanning the width of the prostheca (Figure 6M).

In starving *Campylobacter jejuni* cells, we observed regular filament arrays (Figure 6N). When subjected to environmental or cellular stress some bacteria, including *Escherichia coli* have been shown to reorganize their DNA into protective crystalline arrays (Wolf *et al.*, 1999). Since then, additional nucleoid associated proteins have been identified that organize DNA into higher order

structures in stationary phase or stress conditions (Teramoto *et al.*, 2010, Lim *et al.*, 2013). The structures we observed in *C. jejuni* resemble those seen in *E. coli* cells overexpressing the protective DNA binding protein Dps (Wolf *et al.*, 1999) and may therefore represent such a nucleoprotein array.

Several other proteins have been shown to copolymerize with DNA into filaments for various functions, including RecA (homologous recombination) (Egelman & Stasiak, 1986) and MuB (DNA transposition) (Mizuno *et al.*, 2013). The width of such filaments *in vitro* (~10 nm) is similar to widths we observed in cells; it is possible that some of the structures in Figure 6 represent these DNA-related processes. Other bacterial proteins form filaments to regulate their function, and it has been suggested that this property may have been coopted in the evolution of the cytoskeleton (Barry & Gitai, 2011). We previously observed such filaments of CTP synthase in tomograms of *Caulobacter crescentus* cells (Ingerson-Mahar *et al.*, 2010). Another protein, alcohol dehydrogenase, forms plaited filaments ~10 nm wide, called spiroosomes, in many bacteria capable of anaerobic metabolism (Matayoshi *et al.*, 1989, Laurenceau *et al.*, 2015). It is possible that some of the filament arrays and chains we observed in tomograms may be filaments formed by these or other, yet uncharacterized, proteins.

In addition to filament arrays and bundles, we observed individual or paired filaments in nearly every species imaged. Examples are shown in Figure 7. (Note that due to their ubiquity, statistics are not included in Supplementary Table 1.) Filaments were seen with various orientations in the cytoplasm (Figure 7A-C), as well as running alongside the membrane (Figure D-E). Consistent with our previous work (Swulius *et al.*, 2011), we did not observe any arcing

filaments immediately adjacent to the membrane as predicted by some studies of MreB (e.g. (Jones *et al.*, 2001, Shih *et al.*, 2003)). (Note that we did observe filaments corresponding to the known types of MamK (Komeili *et al.*, 2006, Scheffel *et al.*, 2006), FtsZ (Li *et al.*, 2007, Szwedziak *et al.*, 2014), and bactofilins (Kuhn *et al.*, 2010) but we do not show them here since they have already been characterized.) Paired filaments have been shown to function in plasmid segregation, so it is possible that some paired filaments we observed were such ParM or TubZ structures (Aylett *et al.*, 2010, Bharat *et al.*, 2015).

Tubes

In addition to the known types of tubes we have reported earlier (bacterial microtubules (Pilhofer *et al.*, 2011) and type VI secretion systems (Basler *et al.*, 2012)), we observed several novel tubular structures in bacterial cells (Figure 8). In *Thiomicrospira crunogena* we found large tubes (18.6 ± 1.8 nm diameter) containing eight outer protofilaments surrounding a central protofilament (Figure 8A). *H. neapolitanus* c2 cells also contained large tubes (16.7 ± 0.7 nm diameter) with a central filament (Figure 8B). In several other species, we observed hollow tubes of varying dimensions: 8.9 ± 0.3 nm diameter in *Bdellovibrio bacteriovorus* (Figure 8C), 14.3 ± 1.7 nm in *T. intermedia* (Figure 8D), and 8.3 ± 0.5 nm in *H. neptunium* (Figure 8E). *H. neptunium* cells also contained many rings of similar diameter. In fact, we observed rings in many species, which could be assembly or disassembly intermediates of tubes.

In addition to isolated rings, in one case we observed an organized array of rings. One slightly lysed (a condition that flattens the cell and increases image quality) *H. pylori* cell contained a striking array of about two dozen evenly spaced rings near the cytoplasmic membrane (Figure

8F). Each ring was ~6 nm in diameter and ~20 nm (center-to-center distance) from its neighbors in the square lattice.

Vesicles

In contrast to eukaryotic cells, relatively little is known about membrane remodeling in Bacteria. Compartmentalized cells in the Planktomyces-Verrucomicrobia-Chlamydiae (PVC) superphylum have been shown to contain homologs of eukaryotic membrane trafficking proteins (Santarella-Mellwig *et al.*, 2010) and exhibit endocytosis-like protein uptake (Lonhienne *et al.*, 2010). An additional potential membrane-remodeling system based on FtsZ homologues is more widespread across Bacteria, but its function remains unknown (Makarova & Koonin, 2010).

Despite this limited evidence for membrane remodeling in Bacteria, we observed intracellular vesicles in nearly every species imaged. They exhibited various sizes, shapes, membrane layers, and contents. They were frequently found near the cytoplasmic membrane. Figure 9 shows examples of round and horseshoe-shaped vesicles. Round vesicles were found in nearly every species imaged, and therefore no statistics for them are compiled in Supplementary Table 1. Most round vesicles were empty (density similar to background; e.g. Figure 9A-C). One of these vesicles, observed in a lysed cell (improving clarity by reducing cytoplasmic crowding), exhibited regularly spaced protein densities around its exterior (Figure 9C). Others were at least partially filled with denser material (e.g. Figure 9D-F). In two *M. xanthus* cells overexpressing a fluorescent fusion of a periplasmic protein (PilP-sfGFP), we observed round vesicles containing a dense amorphous core (Figure 9F). These could be a novel form of membrane-bound inclusion

body, perhaps packaged from the periplasm. In eight species, we observed horseshoe-shaped vesicles (Figure 9G-H).

Flattened vesicles (Figure 10A-F) were less common than round vesicles, and were usually observed near membranes or wrapping around storage granules (Figure 10E), suggesting a possible functional relationship. Flattened vesicles were usually empty. One *T. intermedia* cell contained a stack of flattened vesicles (Figure 10A). Flattened vesicles were particularly prevalent in *C. crescentus* cells (Figure 10B-E). *P. debontii* cells contained flattened vesicles that neither ran along the membrane nor wrapped around granules (Figure 10F). Since the lowest energy shape of a liposome is a sphere, it is likely that the vesicles were flattened by cytoplasmic pressure or some other constraint such as associated protein.

Many cells contained nested vesicles, with diverse sizes and shapes, as well as subcellular locations (Figure 10G-L). In some nested vesicles, densities were observed bridging the inner and outer membranes (Figure 10G-H). Cells of strain JT5 exhibited multiple nested vesicles of uniform shape and size (Figure 10L).

We also observed periplasmic vesicles in many species (Figure 11). They were typically empty and exhibited great variability in size, shape, and abundance. In some cases, they were even seen to form branching networks (Figure 11A). As with cytoplasmic vesicles, they were most abundant in cells showing signs of stress.

Conclusions

Here we present the results of a survey of, to our knowledge, uncharacterized bacterial structures that we have observed in our work over the last 10+ years. We hope that further study will identify them and their functions. Already, they signal the wealth of complexity still to be discovered in bacterial cells.

MATERIALS and METHODS

Strains and growth

Unless otherwise noted, bacterial strains were wild-type and grown in species-standard medium and conditions to mid-log or early stationary phase. *Azospirillum brasilense* cultures were switched to nitrogen-free medium for ~16 hours prior to imaging to induce nitrogen fixation and digestion of storage granules that decrease image quality. Predatory *Bdellovibrio bacteriovorus* cells were co-cultured with *Vibrio cholerae* strain MKW1383. *Helicobacter pylori* cells were cultured with human gastric carcinoma cells. In all cases, samples of cells in growth medium were mixed with BSA-treated 10nm colloidal gold fiducials (Sigma), applied to glow-discharged EM grids (Quantifoil), and plunge-frozen in a liquid ethane-propane mixture (Tivol *et al.*, 2008). Grids were maintained at liquid nitrogen temperature throughout storage, transfer, and imaging.

Electron cryotomography

Plunge-frozen samples were imaged using either a Polara or Titan Krios 300 kV FEG transmission electron microscope (FEI Company) equipped with an energy filter (Gatan). Images were recorded using either a lens-coupled 4k x 4k UltraCam CCD (Gatan) or a K2 Summit direct electron detector (Gatan). Tilt-series were recorded from -60° to +60° in 1-2°

increments, with defoci of ~6-12 μm and a cumulative dose of ~100-200 $\text{e}^-/\text{\AA}^2$. Tilt-series were acquired automatically using either Leginon (Suloway *et al.*, 2009) or UCSF Tomography (Zheng *et al.*, 2007) software. Tomographic reconstructions were calculated using either the IMOD software package (Kremer *et al.*, 1996) or Raptor (Amat *et al.*, 2008). 3D segmentations and movies were produced with IMOD (Kremer *et al.*, 1996). Subtomogram averages were calculated using PEET software (Nicastro *et al.*, 2006).

ACKNOWLEDGMENTS

The authors would like to thank our collaborators who provided strains for imaging: Andrew Camilli (*Streptococcus pneumoniae*), Eric Matson (strain JT5), Gladys Alexandre (*Azospirillum brasilense* mutants), Lotte Sogaard-Andersen, Simon Ringgaard and Matthew K. Waldor (*Vibrio cholerae* wild type and mutants), Michael Marletta (*Shewanella putrefaciens*), and Gordon Cannon and Sabine Heinhorst (*Halothiobacillus neapolitanus* and *Thiomonas intermedia*). We also thank members of the Jensen lab for helpful discussions.

COMPETING INTERESTS

No competing interests declared.

AUTHOR CONTRIBUTIONS

Conceptualization: M.J.D. and G.J.J.; formal analysis and investigation: M.J.D., C.M.O., A.P., J.C., K.G., T.J., J.T., J.D., Y.P., A.K., A.I.J., M.P., S.C., E.I.T., Y.-W.C., A.B., J.S., Z.L., P.S., C.V.I., B.A.S., A.W.M.; writing – original draft preparation: M.J.D. and C.M.O.; writing –

review and editing: M.J.D., C.M.O., G.J.J.; funding acquisition: M.J.D. and G.J.J.; resources: G.J.J.; supervision: M.J.D. and G.J.J.

FUNDING

This work was supported by the Hampshire College Dr. Lucy fund and the Collaborative Modeling Center, the NIH grant R01 AI27401 to GJJ, the Beckman Institute at Caltech, the Gordon and Betty Moore Foundation, the Human Frontier Science Program, the Howard Hughes Medical Institute, and the John Templeton Foundation as part of the Boundaries of Life project. The opinions expressed in this publication are those of the authors and do not necessarily reflect the views of the John Templeton Foundation.

REFERENCES

- Abrusci, P., M. Vergara-Irigaray, S. Johnson, M.D. Beeby, D.R. Hendrixson, P. Roversi, M.E. Friede, J.E. Deane, G.J. Jensen, C.M. Tang & S.M. Lea, (2013) Architecture of the major component of the type III secretion system export apparatus. *Nature structural & molecular biology* **20**: 99-104.
- Amat, F., F. Moussavi, L.R. Comolli, G. Elidan, K.H. Downing & M. Horowitz, (2008) Markov random field based automatic image alignment for electron tomography. *J Struct Biol* **161**: 260-275.
- Aylett, C.H., Q. Wang, K.A. Michie, L.A. Amos & J. Lowe, (2010) Filament structure of bacterial tubulin homologue TubZ. *Proc Natl Acad Sci U S A* **107**: 19766-19771.
- Barry, R.M. & Z. Gitai, (2011) Self-assembling enzymes and the origins of the cytoskeleton. *Current opinion in microbiology* **14**: 704-711.
- Basler, M., M. Pilhofer, G.P. Henderson, G.J. Jensen & J.J. Mekalanos, (2012) Type VI secretion requires a dynamic contractile phage tail-like structure. *Nature* **483**: 182-186.
- Beeby, M., J.C. Gumbart, B. Roux & G.J. Jensen, (2013) Architecture and assembly of the Gram-positive cell wall. *Mol Microbiol* **88**: 664-672.
- Bharat, T.A., G.N. Murshudov, C. Sachse & J. Lowe, (2015) Structures of actin-like ParM filaments show architecture of plasmid-segregating spindles. *Nature*: 1-5.

- 372 Bible, A., M.H. Russell & G. Alexandre, (2012) The *Azospirillum brasilense* Che1 chemotaxis
373 pathway controls swimming velocity, which affects transient cell-to-cell clumping. *J*
374 *Bacteriol* **194**: 3343-3355.
- 375 Bible, A.N., G.K. Khalsa-Moyers, T. Mukherjee, C.S. Green, P. Mishra, A. Purcell, A.
376 Aksenova, G.B. Hurst & G. Alexandre, (2015) Metabolic adaptations of *Azospirillum*
377 *brasilense* to oxygen stress by cell-to-cell clumping and flocculation. *Appl Environ*
378 *Microbiol* **81**: 8346-8357.
- 379 Briegel, A., H.J. Ding, Z. Li, J. Werner, Z. Gitai, D.P. Dias, R.B. Jensen & G.J. Jensen, (2008)
380 Location and architecture of the *Caulobacter crescentus* chemoreceptor array. *Mol*
381 *Microbiol* **69**: 30-41.
- 382 Briegel, A., X. Li, A.M. Bilwes, K.T. Hughes, G.J. Jensen & B.R. Crane, (2012) Bacterial
383 chemoreceptor arrays are hexagonally packed trimers of receptor dimers networked by
384 rings of kinase and coupling proteins. *Proc Natl Acad Sci U S A* **109**: 3766-3771.
- 385 Cameron, D.E., J.M. Urbach & J.J. Mekalanos, (2008) A defined transposon mutant library and
386 its use in identifying motility genes in *Vibrio cholerae*. *Proc Natl Acad Sci U S A* **105**:
387 8736-8741.
- 388 Chang, Y.W., S. Chen, E.I. Tocheva, A. Treuner-Lange, S. Lobach, L. Sogaard-Andersen & G.J.
389 Jensen, (2014) Correlated cryogenic photoactivated localization microscopy and cryo-
390 electron tomography. *Nature methods* **11**: 737-739.
- 391 Chang, Y.W., L.A. Rettberg, A. Treuner-Lange, J. Iwasa, L. Sogaard-Andersen & G.J. Jensen,
392 (2016) Architecture of the type IVa pilus machine. *Science* **351**: aad2001.
- 393 Chen, S., M. Beeby, G.E. Murphy, J.R. Leadbetter, D.R. Hendrixson, A. Briegel, Z. Li, J. Shi,
394 E.I. Tocheva, A. Muller, M.J. Dobro & G.J. Jensen, (2011) Structural diversity of
395 bacterial flagellar motors. *The EMBO journal* **30**: 2972-2981.
- 396 Crowley, J.T., A.M. Toledo, T.J. LaRocca, J.L. Coleman, E. London & J.L. Benach, (2013)
397 Lipid exchange between *Borrelia burgdorferi* and host cells. *PLoS Pathog* **9**: e1003109.
- 398 De Troch, P. & J. Vanderleyden, (1996) Surface Properties and Motility of *Rhizobium* and
399 *Azospirillum* in Relation to Plant Root Attachment. *Microb Ecol* **32**: 149-169.
- 400 Ding, H.J., C.M. Oikonomou & G.J. Jensen, (2015) The Caltech Tomography Database and
401 Automatic Processing Pipeline. *J Struct Biol* **192**: 279-286.
- 402 Dueholm, M.S., M. Albertsen, D. Otzen & P.H. Nielsen, (2012) Curli functional amyloid
403 systems are phylogenetically widespread and display large diversity in operon and
404 protein structure. *PLoS One* **7**: e51274.
- 405 Ebersbach, G., A. Briegel, G.J. Jensen & C. Jacobs-Wagner, (2008) A self-associating protein
406 critical for chromosome attachment, division, and polar organization in *caulobacter*. *Cell*
407 **134**: 956-968.

408 Egelman, E.H. & A. Stasiak, (1986) Structure of helical RecA-DNA complexes. Complexes
409 formed in the presence of ATP-gamma-S or ATP. *J Mol Biol* **191**: 677-697.

410 Epstein, E.A., M.A. Reizian & M.R. Chapman, (2009) Spatial clustering of the curlin secretion
411 lipoprotein requires curli fiber assembly. *J Bacteriol* **191**: 608-615.

412 Gan, L., S. Chen & G.J. Jensen, (2008) Molecular organization of Gram-negative peptidoglycan.
413 *Proc Natl Acad Sci U S A* **105**: 18953-18957.

414 Guerrero-Ferreira, R.C., P.H. Viollier, B. Ely, J.S. Poindexter, M. Georgieva, G.J. Jensen & E.R.
415 Wright, (2011) Alternative mechanism for bacteriophage adsorption to the motile
416 bacterium *Caulobacter crescentus*. *Proc Natl Acad Sci U S A* **108**: 9963-9968.

417 Iancu, C.V., H.J. Ding, D.M. Morris, D.P. Dias, A.D. Gonzales, A. Martino & G.J. Jensen,
418 (2007) The structure of isolated *Synechococcus* strain WH8102 carboxysomes as
419 revealed by electron cryotomography. *J Mol Biol* **372**: 764-773.

420 Ingerson-Mahar, M., A. Briegel, J.N. Werner, G.J. Jensen & Z. Gitai, (2010) The metabolic
421 enzyme CTP synthase forms cytoskeletal filaments. *Nature cell biology* **12**: 739-746.

422 Jones, L.J., R. Carballido-Lopez & J. Errington, (2001) Control of cell shape in bacteria: helical,
423 actin-like filaments in *Bacillus subtilis*. *Cell* **104**: 913-922.

424 Komeili, A., Z. Li, D.K. Newman & G.J. Jensen, (2006) Magnetosomes are cell membrane
425 invaginations organized by the actin-like protein MamK. *Science* **311**: 242-245.

426 Koster, A.J., R. Grimm, D. Typke, R. Hegerl, A. Stoschek, J. Walz & W. Baumeister, (1997)
427 Perspectives of molecular and cellular electron tomography. *J Struct Biol* **120**: 276-308.

428 Kremer, J.R., D.N. Mastronarde & J.R. McIntosh, (1996) Computer visualization of three-
429 dimensional image data using IMOD. *J Struct Biol* **116**: 71-76.

430 Kuhn, J., A. Briegel, E. Morschel, J. Kahnt, K. Leser, S. Wick, G.J. Jensen & M. Thanbichler,
431 (2010) Bactofilins, a ubiquitous class of cytoskeletal proteins mediating polar localization
432 of a cell wall synthase in *Caulobacter crescentus*. *The EMBO journal* **29**: 327-339.

433 Kulp, A. & M.J. Kuehn, (2010) Biological functions and biogenesis of secreted bacterial outer
434 membrane vesicles. *Annu Rev Microbiol* **64**: 163-184.

435 Laurenceau, R., P.V. Krasteva, A. Diallo, S. Ouarti, M. Duchateau, C. Malosse, J. Chamot-
436 Rooke & R. Fronzes, (2015) Conserved *Streptococcus pneumoniae* spiroosomes suggest a
437 single type of transformation pilus in competence. *PLoS Pathog* **11**: e1004835.

438 Li, Z., M.J. Trimble, Y.V. Brun & G.J. Jensen, (2007) The structure of FtsZ filaments in vivo
439 suggests a force-generating role in cell division. *The EMBO journal* **26**: 4694-4708.

440 Lim, C.J., S.Y. Lee, J. Teramoto, A. Ishihama & J. Yan, (2013) The nucleoid-associated protein
441 Dan organizes chromosomal DNA through rigid nucleoprotein filament formation in E.
442 coli during anoxia. *Nucleic Acids Res* **41**: 746-753.

443 Lonhienne, T.G., E. Sagulenko, R.I. Webb, K.C. Lee, J. Franke, D.P. Devos, A. Nouwens, B.J.
444 Carroll & J.A. Fuerst, (2010) Endocytosis-like protein uptake in the bacterium *Gemmata*
445 *obscuriglobus*. *Proc Natl Acad Sci U S A* **107**: 12883-12888.

446 Makarova, K.S. & E.V. Koonin, (2010) Two new families of the FtsZ-tubulin protein
447 superfamily implicated in membrane remodeling in diverse bacteria and archaea. *Biol*
448 *Direct* **5**: 33.

449 Matayoshi, S., H. Oda & G. Sarwar, (1989) Relationship between the production of spiroosomes
450 and anaerobic glycolysis activity in *Escherichia coli* B. *J Gen Microbiol* **135**: 525-529.

451 Mizuno, N., M. Dramicanin, M. Mizuuchi, J. Adam, Y. Wang, Y.W. Han, W. Yang, A.C.
452 Steven, K. Mizuuchi & S. Ramon-Maiques, (2013) MuB is an AAA+ ATPase that forms
453 helical filaments to control target selection for DNA transposition. *Proc Natl Acad Sci U*
454 *S A* **110**: E2441-2450.

455 Moissl, C., R. Rachel, A. Briegel, H. Engelhardt & R. Huber, (2005) The unique structure of
456 archaeal 'hami', highly complex cell appendages with nano-grappling hooks. *Mol*
457 *Microbiol* **56**: 361-370.

458 Mukherjee, T., D. Kumar, N. Burriss, Z. Xie & G. Alexandre, (2016) *Azospirillum brasilense*
459 Chemotaxis Depends on Two Signaling Pathways Regulating Distinct Motility
460 Parameters. *J Bacteriol* **198**: 1764-1772.

461 Muller, A., M. Beeby, A.W. McDowall, J. Chow, G.J. Jensen & W.M. Clemons, Jr., (2014)
462 Ultrastructure and complex polar architecture of the human pathogen *Campylobacter*
463 *jejuni*. *MicrobiologyOpen* **3**: 702-710.

464 Murphy, G.E., J.R. Leadbetter & G.J. Jensen, (2006) In situ structure of the complete *Treponema*
465 *primitia* flagellar motor. *Nature* **442**: 1062-1064.

466 Murphy, G.E., E.G. Matson, J.R. Leadbetter, H.C. Berg & G.J. Jensen, (2008) Novel
467 ultrastructures of *Treponema primitia* and their implications for motility. *Mol Microbiol*
468 **67**: 1184-1195.

469 Nicastro, D., C. Schwartz, J. Pierson, R. Gaudette, M.E. Porter & J.R. McIntosh, (2006) The
470 molecular architecture of axonemes revealed by cryoelectron tomography. *Science* **313**:
471 944-948.

472 Oikonomou, C.M. & G.J. Jensen, (2016) A new view into prokaryotic cell biology from electron
473 cryotomography. *Nat Rev Microbiol* **14**: 205-220.

474 Pilhofer, M., M.S. Ladinsky, A.W. McDowall & G.J. Jensen, (2010) Bacterial TEM: new
475 insights from cryo-microscopy. *Methods in cell biology* **96**: 21-45.

476 Pilhofer, M., M.S. Ladinsky, A.W. McDowall, G. Petroni & G.J. Jensen, (2011) Microtubules in
477 bacteria: Ancient tubulins build a five-protofilament homolog of the eukaryotic
478 cytoskeleton. *PLoS biology* **9**: e1001213.

479 Pirbadian, S., S.E. Barchinger, K.M. Leung, H.S. Byun, Y. Jangir, R.A. Bouhenni, S.B. Reed,
480 M.F. Romine, D.A. Saffarini, L. Shi, Y.A. Gorby, J.H. Golbeck & M.Y. El-Naggar,
481 (2014) Shewanella oneidensis MR-1 nanowires are outer membrane and periplasmic
482 extensions of the extracellular electron transport components. *Proc Natl Acad Sci U S A*
483 **111**: 12883-12888.

484 Pommier, Y., J.M. Covey, D. Kerrigan, J. Markovits & R. Pham, (1987) DNA unwinding and
485 inhibition of mouse leukemia L1210 DNA topoisomerase I by intercalators. *Nucleic*
486 *Acids Res* **15**: 6713-6731.

487 Remis, J.P., D. Wei, A. Gorur, M. Zemla, J. Haraga, S. Allen, H.E. Witkowska, J.W. Costerton,
488 J.E. Berleman & M. Auer, (2014) Bacterial social networks: structure and composition of
489 Myxococcus xanthus outer membrane vesicle chains. *Environ Microbiol* **16**: 598-610.

490 Ruska, E., (1987) Nobel lecture. The development of the electron microscope and of electron
491 microscopy. *Biosci Rep* **7**: 607-629.

492 Santarella-Mellwig, R., J. Franke, A. Jaedicke, M. Gorjanacz, U. Bauer, A. Budd, I.W. Mattaj &
493 D.P. Devos, (2010) The compartmentalized bacteria of the planctomycetes-
494 verrucomicrobia-chlamydiae superphylum have membrane coat-like proteins. *PLoS*
495 *biology* **8**: e1000281.

496 Scheffel, A., M. Gruska, D. Faivre, A. Linaroudis, J.M. Plitzko & D. Schuler, (2006) An acidic
497 protein aligns magnetosomes along a filamentous structure in magnetotactic bacteria.
498 *Nature* **440**: 110-114.

499 Shetty, A., S. Chen, E.I. Tocheva, G.J. Jensen & W.J. Hickey, (2011) Nanopods: a new bacterial
500 structure and mechanism for deployment of outer membrane vesicles. *PLoS One* **6**:
501 e20725.

502 Shih, Y.L., T. Le & L. Rothfield, (2003) Division site selection in Escherichia coli involves
503 dynamic redistribution of Min proteins within coiled structures that extend between the
504 two cell poles. *Proc Natl Acad Sci U S A* **100**: 7865-7870.

505 Skare, J.T., E.S. Shang, D.M. Foley, D.R. Blanco, C.I. Champion, T. Mirzabekov, Y. Sokolov,
506 B.L. Kagan, J.N. Miller & M.A. Lovett, (1995) Virulent strain associated outer
507 membrane proteins of Borrelia burgdorferi. *J Clin Invest* **96**: 2380-2392.

508 Steenhoudt, O. & J. Vanderleyden, (2000) Azospirillum, a free-living nitrogen-fixing bacterium
509 closely associated with grasses: genetic, biochemical and ecological aspects. *FEMS*
510 *Microbiol Rev* **24**: 487-506.

- 511 Suloway, C., J. Shi, A. Cheng, J. Pulokas, B. Carragher, C.S. Potter, S.Q. Zheng, D.A. Agard &
512 G.J. Jensen, (2009) Fully automated, sequential tilt-series acquisition with Legion. *J*
513 *Struct Biol* **167**: 11-18.
- 514 Swulius, M.T., S. Chen, H. Jane Ding, Z. Li, A. Briegel, M. Pilhofer, E.I. Tocheva, S.R.
515 Lybarger, T.L. Johnson, M. Sandkvist & G.J. Jensen, (2011) Long helical filaments are
516 not seen encircling cells in electron cryotomograms of rod-shaped bacteria. *Biochemical*
517 *and biophysical research communications* **407**: 650-655.
- 518 Swulius, M.T. & G.J. Jensen, (2012) The helical MreB cytoskeleton in Escherichia coli
519 MC1000/pLE7 is an artifact of the N-Terminal yellow fluorescent protein tag. *J Bacteriol*
520 **194**: 6382-6386.
- 521 Szwedziak, P., Q. Wang, T.A. Bharat, M. Tsim & J. Lowe, (2014) Architecture of the ring
522 formed by the tubulin homologue FtsZ in bacterial cell division. *eLife* **4**.
- 523 Teramoto, J., S.H. Yoshimura, K. Takeyasu & A. Ishihama, (2010) A novel nucleoid protein of
524 Escherichia coli induced under anaerobic growth conditions. *Nucleic Acids Res* **38**:
525 3605-3618.
- 526 Tivol, W.F., A. Briegel & G.J. Jensen, (2008) An improved cryogen for plunge freezing.
527 *Microscopy and microanalysis : the official journal of Microscopy Society of America,*
528 *Microbeam Analysis Society, Microscopical Society of Canada* **14**: 375-379.
- 529 Tocheva, E.I., E.G. Matson, D.M. Morris, F. Moussavi, J.R. Leadbetter & G.J. Jensen, (2011)
530 Peptidoglycan remodeling and conversion of an inner membrane into an outer membrane
531 during sporulation. *Cell* **146**: 799-812.
- 532 Van Gerven, N., R.D. Klein, S.J. Hultgren & H. Remaut, (2015) Bacterial amyloid formation:
533 structural insights into curli biogenesis. *Trends Microbiol* **23**: 693-706.
- 534 Weiner, R.M., M. Melick, K. O'Neill & E. Quintero, (2000) Hyphomonas adhaerens sp. nov.,
535 Hyphomonas johnsonii sp. nov. and Hyphomonas rosenbergii sp. nov., marine budding
536 and prosthecate bacteria. *Int J Syst Evol Microbiol* **50 Pt 2**: 459-469.
- 537 Wolf, S.G., D. Frenkiel, T. Arad, S.E. Finkel, R. Kolter & A. Minsky, (1999) DNA protection by
538 stress-induced biocrystallization. *Nature* **400**: 83-85.
- 539 Zerfas, P.M., M. Kessel, E.J. Quintero & R.M. Weiner, (1997) Fine-structure evidence for cell
540 membrane partitioning of the nucleoid and cytoplasm during bud formation in
541 Hyphomonas species. *J Bacteriol* **179**: 148-156.
- 542 Zheng, S.Q., B. Keszthelyi, E. Branlund, J.M. Lyle, M.B. Braunfeld, J.W. Sedat & D.A. Agard,
543 (2007) UCSF tomography: an integrated software suite for real-time electron microscopic
544 tomographic data collection, alignment, and reconstruction. *J Struct Biol* **157**: 138-147.

FIGURE LEGENDS

Figure 1. Novel *Prosthecobacter debontii* appendages. Multiple external appendages (arrowheads) were observed by ECT on *P. debontii* prosthecae (**A**). A central tomographic slice is shown, with a single appendage enlarged in the inset. Subtomogram averaging revealed the structure in more detail. Side (above) and top (below) views in (**B**) show the characteristic disc-like densities and the five legs attaching to the cell surface. The red box shows which view was used to rotate the image 90° for the bottom image. (**C**) shows a 3D isosurface of the average, seen from the side and top (inset). Scale bars 50 nm in (**A**) and 20 nm in inset.

Figure 2. Novel *Azospirillum brasilense* hooks. Many hook-like structures were observed on the surface of *A. brasilense* cells. A central tomographic slice is shown, with arrowheads indicating hooks. A single hook is shown enlarged at right. Scale bar 50 nm.

Figure 3. Strain JT5 fimbriae. (**A-C**) show slices at progressive z-heights through a cryotomogram of a cell of strain JT5 (related to the *Dysgonomonas* genus). Abundant fimbriae can be seen at the cell pole. Scale bars 100 nm.

Figure 4. Vesicular outer membrane chains in *Borrelia burgdorferi*. Central tomographic slices of two different *B. burgdorferi* cells illustrate the chained vesicle (**A**) and tubular (**B**) morphologies of membrane-derived structures. V indicates vesicles; F indicates periplasmic flagella. Scale bars 100 nm.

Figure 5. Novel *Vibrio cholerae* nanospheres. Clusters of “nanospheres” were observed in three cryotomograms of *V. cholerae* cells (central slices shown in **A-C**). N indicates nanospheres; A indicates associated filament array. **(D)** shows a segmentation of the cluster seen in **(C)** overlaid on the tomographic slice, with outer and inner membranes in magenta and cyan, respectively, and nanospheres in green. **(E)** shows a clipping plane through the 3D segmentation revealing the thick walls and hollow centers of the nanospheres. Scale bars 100 nm.

Figure 6. Filament bundles, arrays, and chains. *Hyphomonas neptunium* division stalks contained helical bundles **(A)** that straightened when cells were treated with ethidium bromide **(B)**. The right side of panel **(A)** shows a 3D segmentation of the helical bundle, with side and top views of subtomogram averaged insets. Labeled dimensions are in nanometers. **(C)** Large filament bundles in *Helicobacter pylori*. **(D)** A long mesh-like filament array in *Vibrio cholerae*, with segmentation at right. **(E)** A more typical *V. cholerae* filament array. Filament arrays in *Thiomonas intermedia* **(F)**, *Hyphomonas neptunium* **(G)** *Hylemonella gracilis* **(H)**, *Halothiobacillus neapolitanus* c2 **(I)**, and *Mycobacterium smegmatis* **(J)**. **(K)** A chain in *Prostheco bacter vanneervanii*. **(L-M)** Filament arrays in *Prostheco bacter debontii*. **(N)** A filament array in a starved *Campylobacter jejuni* cell. Scale bars 100 nm (**A-B**, **D-J**, **L-N**) and 50 nm (**C,K**).

Figure 7. Single and paired filaments. Tomographic slices showing paired filaments in *Campylobacter jejuni* **(A)**, and *Thiomicrospira crunogena* **(B)**, and membrane-aligned filaments in *Shewanella putrefaciens* **(C)**, *Prostheco bacter debontii* **(D)**, and *Prostheco bacter fluviatilis*

(E, red arrow shows filament just under the inner membrane). Scale bars 100 nm (A-D) and 50 nm (E).

Figure 8. Tubes and rings. Tubes observed in *Thiomicrospira crunogena* (A), *Halothiobacillus neapolitanus* c2 (B), *Bdellovibrio bacteriovorus* (C), *Thiomonas intermedia* (D), and *Hyphomonas neptunium* (E). In each panel, tomographic slices show a side view (above), and a top view (bottom). (F) An array of rings observed in *Helicobacter pylori*. Scale bars 10 nm (A,C,E), 20 nm (B,D), and 100 nm (F).

Figure 9. Round and horseshoe-shaped vesicles. Tomographic slices showing examples of round vesicles in *Escherichia coli* (A, segmentation shown at right), *Helicobacter pylori* (B), *Helicobacter hepaticus* (C), *Myxococcus xanthus* (D), *Caulobacter crescentus* (E), and *Myxococcus xanthus* overexpressing PilP-sfGFP (F). Examples of horseshoe-shaped vesicles in *Ralstonia eutropha* (G) and *Prostheco bacter fluviatilis* (H), with 3D segmentations shown at right. In the segmentation in (A), outer and inner membranes are in magenta and cyan, respectively, and vesicles in green. Scale bars 50 nm.

Figure 10. Flattened and nested vesicles. Examples of flattened vesicles in *Thiomonas intermedia* (A), *Caulobacter crescentus* (B-E) and *Prostheco bacter debontii* (F). Note storage granules in (E and F), shown in orange in the segmentation in (E). Examples of nested vesicles in *Serpens flexibilis* (G), *Caulobacter crescentus* (H), *Borrelia burgdorferi* (I), *Vibrio cholerae* (J), *Caulobacter crescentus* with segmentation (K), and strain JT5 (L). Inset in (L) shows an enlargement of central vesicle, and a 3D segmentation of the visible portion of the cell is shown

below. In segmentations, outer and inner membranes are shown in magenta and cyan, respectively, and vesicles in green. Scale bars 50 nm.

Figure 11. Periplasmic vesicles. Examples of periplasmic vesicles in *Caulobacter crescentus* (A), *Helicobacter pylori* (B), *Brucella abortus* (C), *Thiomonas intermedia* (D), *Hyphomonas neptunium* (E), *Myxococcus xanthus* (F), and *Halothiobacillus neapolitanus* c2 (G). In each panel, a central tomographic slice is shown, as well as a segmentation with outer and inner membranes in magenta and cyan, respectively, and vesicles in green. Scale bars 50 nm (A-F) and 100 nm (G).

Supplementary Movies 1-11. The movies show all figure panels going slice-by-slice through the Z-stack of the tomogram. Accompanying models are provided when a three-dimensional view is helpful for interpreting the structure. <https://figshare.com/s/782461843c3150d27cfa>

Supplementary Table 1. Species range and frequency of structures observed. For species with many tomograms imaged we are reporting the lowest estimate for counts since not all tomograms were viewed in search of each feature.

Feature	Species	# Tomograms	% Tomograms
Surface appendages	<i>Prostheco bacter debontii</i>	6	4.6
Surface hooks	<i>Azospirillum brasilense</i> WT	20	95.2
	<i>A. brasilense</i> ΔcheOp1	24	92.3
	<i>A. brasilense</i> ΔcheOp4	9	52.9
	<i>A. brasilense</i> ΔcheOp1 ΔcheOp4	0	0.0
Polar fimbriae	Strain JT5 (<i>Dysgonomonas</i>)	41	100
OMV chains	<i>Borrelia burgdorferi</i>	24	52.2
Nanospheres	<i>Vibrio cholerae</i>	3	0.2
Filament bundles	<i>Agrobacterium tumefaciens</i>	1	< 0.1
	<i>Borrelia burgdorferi</i>	1	2.2
	<i>Campylobacter jejuni</i>	2	3.3
	<i>Caulobacter crescentus</i>	1	< 0.1
	<i>Escherichia coli</i>	1	0.1

	<i>Halothiobacillus neapolitanus</i> c2	5	2.6
	<i>Helicobacter pylori</i>	2	2.1
	<i>Hylemonella gracilis</i>	1	0.9
	<i>Hyphomonas neptunium</i>	32	2.7
	<i>Mycobacterium smegmatis</i>	5	5.8
	<i>Myxococcus xanthus</i>	1	0.1
	<i>Prostheco bacter debontii</i>	2	1.5
	<i>Prostheco bacter fluviatilis</i>	5	3.6
	<i>Prostheco bacter vanneervanii</i>	4	2.3
	<i>Thiomonas intermedia</i>	3	6.7
	<i>Vibrio cholerae</i>	10	0.8
	<i>Shewanella putrefaciens</i>	1	6.3
Tubes	<i>Bdellovibrio bacteriovorus</i>	1	0.3
	<i>Halothiobacillus neapolitanus</i> c2	1	0.5
	<i>Hyphomonas neptunium</i>	7	0.6
	<i>Prostheco bacter vanneervanii</i>	1	0.6
	<i>Thiomicrospira crunogena</i>	2	9.1
	<i>Thiomonas intermedia</i>	1	2.2
Ring array	<i>Helicobacter pylori</i>	1	1.0
Vesicles - horseshoe	<i>Caulobacter crescentus</i>	8	0.4
	<i>Hyphomonas neptunium</i>	1	0.1
	<i>Magnetospirillum magneticum</i>	1	0.2
	<i>Myxococcus xanthus</i>	2	0.1
	<i>Prostheco bacter fluviatilis</i>	2	1.4
	<i>Prostheco bacter vanneervanii</i>	1	0.6
	<i>Ralstonia eutropha</i>	1	1.6
	<i>Thiomonas intermedia</i>	2	4.4
Vesicles - flattened	<i>Agrobacterium tumefaciens</i>	1	< 0.1
	<i>Caulobacter crescentus</i>	78	3.6
	<i>Escherichia coli</i>	1	0.1
	<i>Helicobacter pylori</i>	16	2.9
	<i>Hyphomonas neptunium</i>	1	0.1
	<i>Myxococcus xanthus</i>	9	0.5
	<i>Prostheco bacter debontii</i>	1	0.8
	<i>Prostheco bacter dejongeii</i>	7	5.3
	<i>Prostheco bacter fluviatilis</i>	4	2.9
	<i>Prostheco bacter vanneervanii</i>	1	0.6
	<i>Streptococcus pneumoniae</i>	4	11.4
	<i>Thiomonas intermedia</i>	1	2.2
	<i>Treponema primitia</i>	1	1.1
	<i>Vibrio cholerae</i>	3	0.2
Vesicles - nested	<i>Agrobacterium tumefaciens</i>	2	0.1
	<i>Bacillus subtilis</i>	1	1.9
	<i>Bdellovibrio bacteriovorus</i>	1	0.3
	<i>Borrelia burgdorferi</i>	1	2.2

	<i>Brucella abortus</i>	2	3.7
	<i>Caulobacter crescentus</i>	53	2.4
	<i>Escherichia coli</i>	4	0.3
	<i>Halothiobacillus neapolitanus</i> c2	5	2.6
	<i>Helicobacter hepaticus</i>	2	6.1
	<i>Helicobacter pylori</i>	10	1.8
	<i>Hyphomonas neptunium</i>	3	0.3
	Strain JT5 (<i>Dysgonomonas</i>)	2	4.7
	<i>Myxococcus xanthus</i>	23	1.3
	<i>Prostheco bacter debontii</i>	3	2.3
	<i>Prostheco bacter dejongei</i>	3	2.3
	<i>Prostheco bacter fluviatilis</i>	1	0.7
	<i>Prostheco bacter vanneerveni</i>	2	1.1
	<i>Ralstonia eutropha</i>	2	3.2
	<i>Serpens flexibilis</i>	1	10.0
	<i>Sphingopyxis alaskensis</i>	1	4.5
	<i>Streptococcus pneumoniae</i>	1	2.9
	<i>Tetrasphaera remis</i>	1	25.0
	<i>Thiomonas intermedia</i>	1	2.2
Vesicles - periplasmic	<i>Agrobacterium tumefaciens</i>	2	0.1
	<i>Bdellovibrio bacteriovorus</i>	2	0.6
	<i>Brucella abortus</i>	3	5.6
	<i>Campylobacter jejuni</i>	1	1.7
	<i>Caulobacter crescentus</i>	16	0.7
	<i>Escherichia coli</i>	6	0.5
	<i>Halothiobacillus neapolitanus</i>	22	11.5
	<i>Helicobacter hepaticus</i>	2	6.1
	<i>Helicobacter pylori</i>	3	0.5
	<i>Hyphomonas neptunium</i>	3	0.3
	<i>Myxococcus xanthus</i>	1	0.1
	<i>Prostheco bacter dejongei</i>	1	0.8
	<i>Prostheco bacter fluviatilis</i>	2	1.4
	<i>Prostheco bacter vanneerveni</i>	3	1.7
	<i>Ruminococcus flavefaciens</i>	2	18.2
	<i>Thiomicrospira crunogena</i>	1	4.5
	<i>Thiomonas intermedia</i>	1	2.2
	<i>Vibrio cholerae</i>	2	0.2

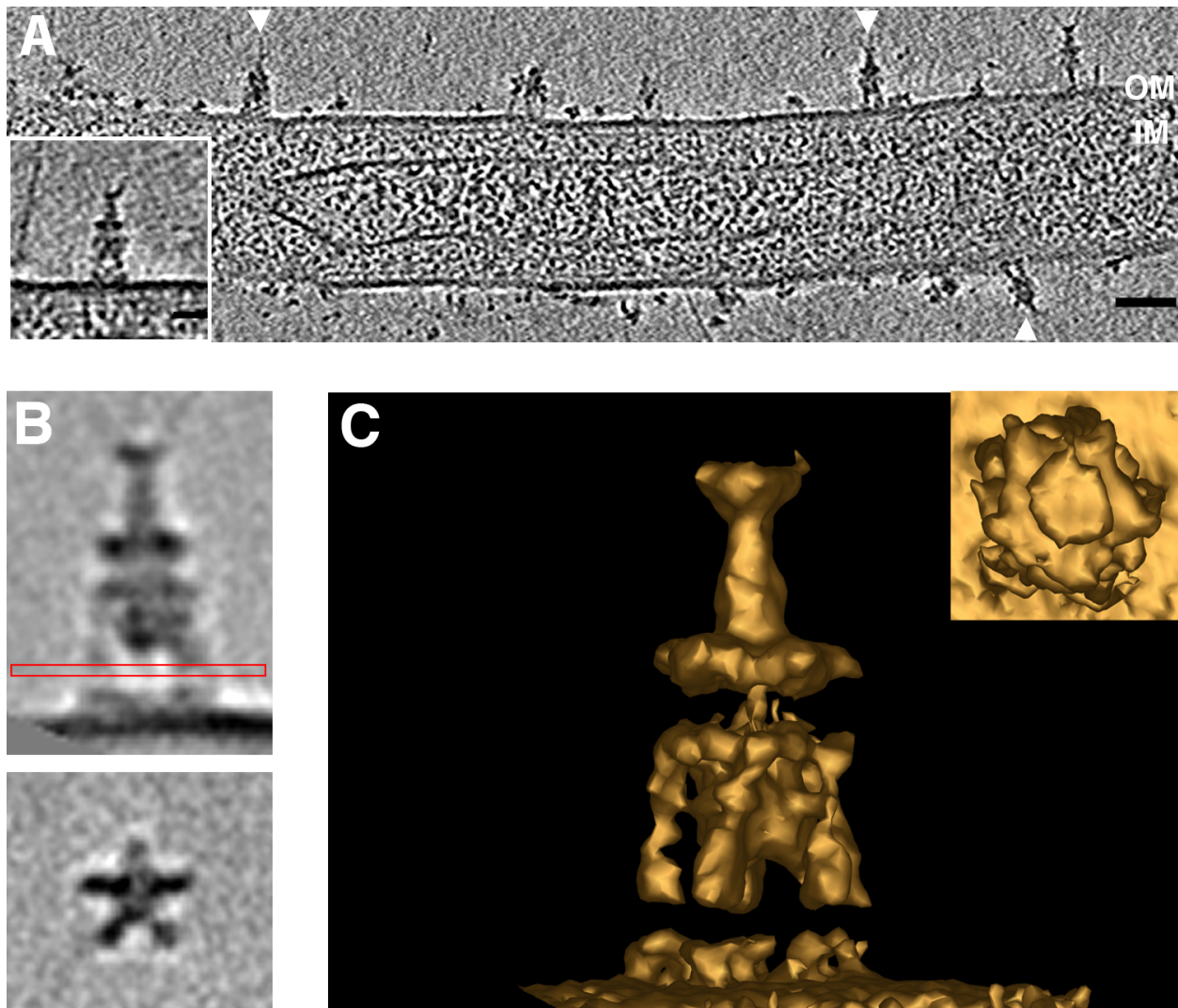


Figure 1

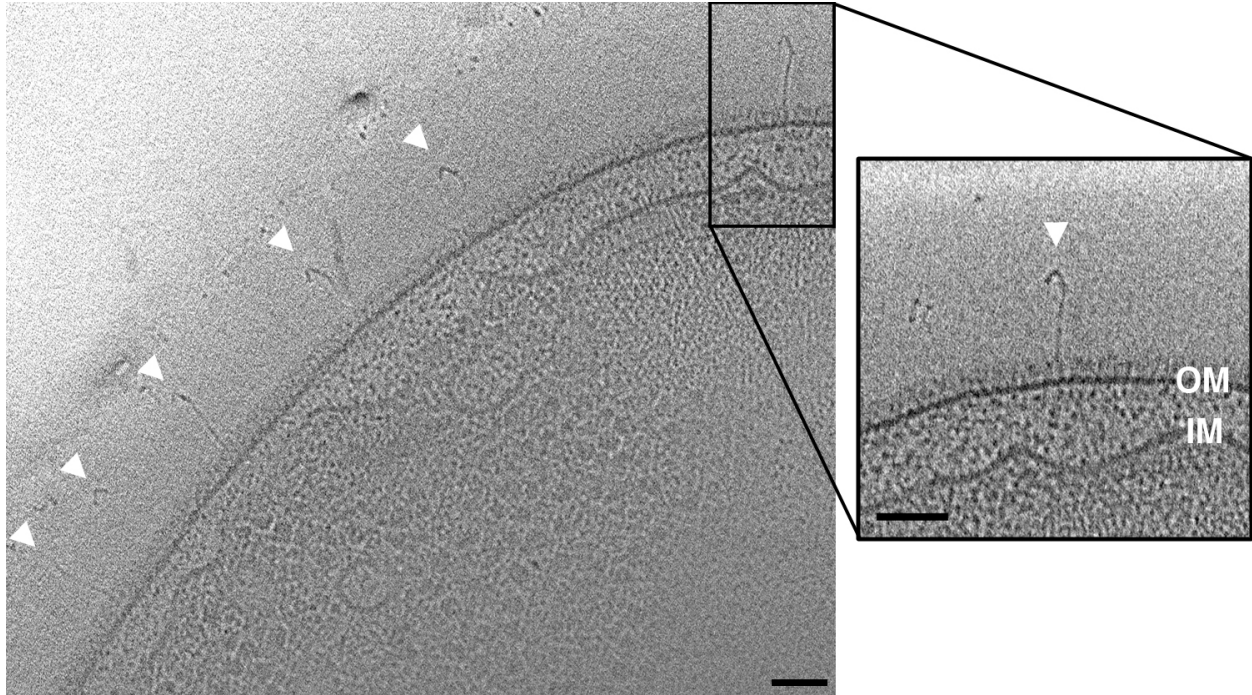


Figure 2

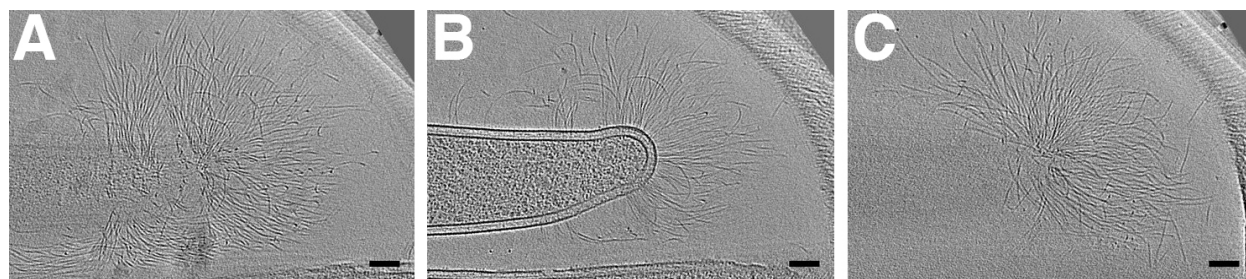


Figure 3

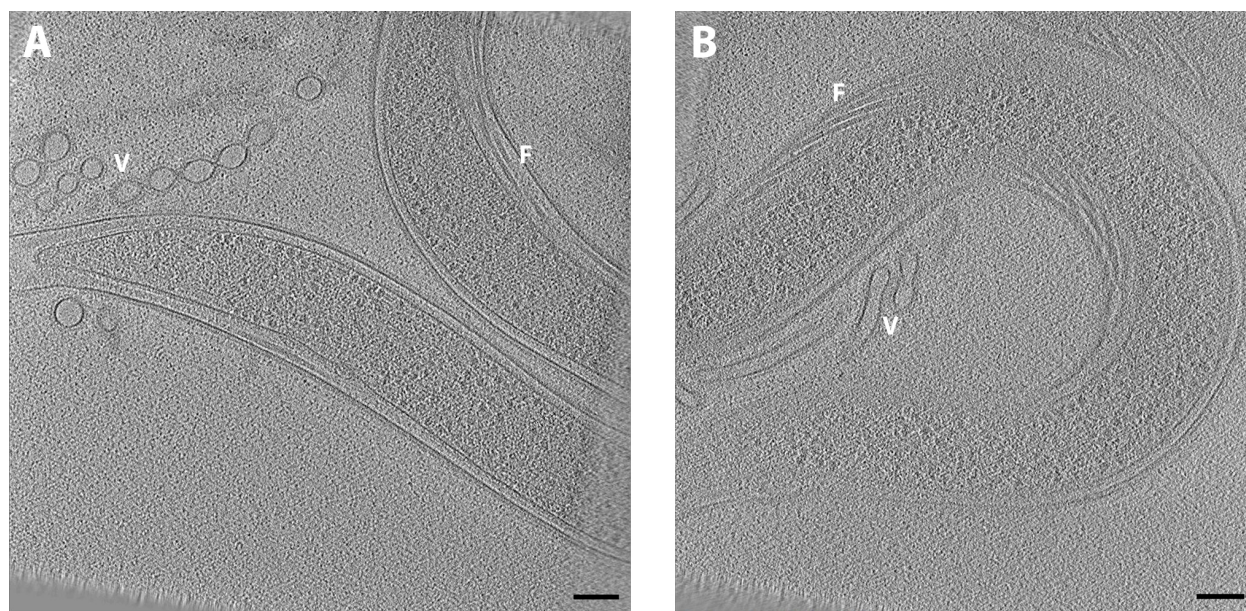


Figure 4

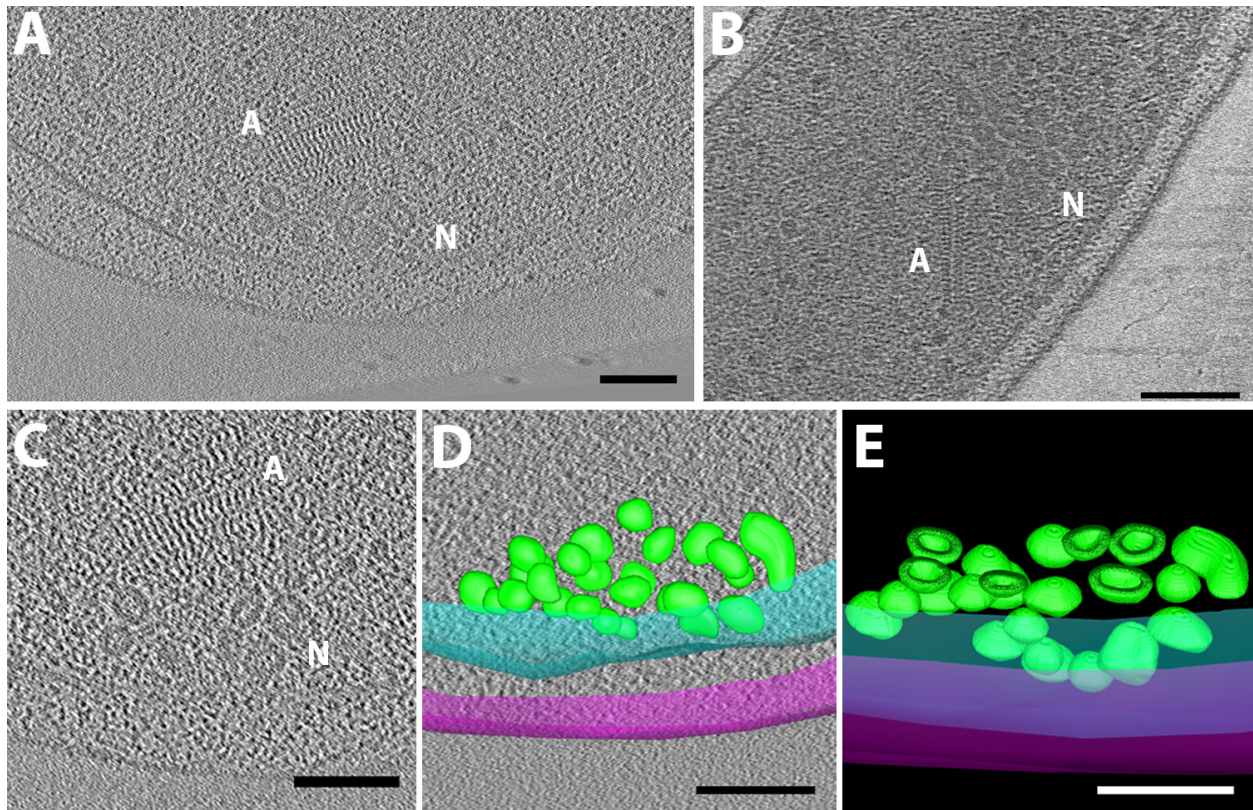


Figure 5

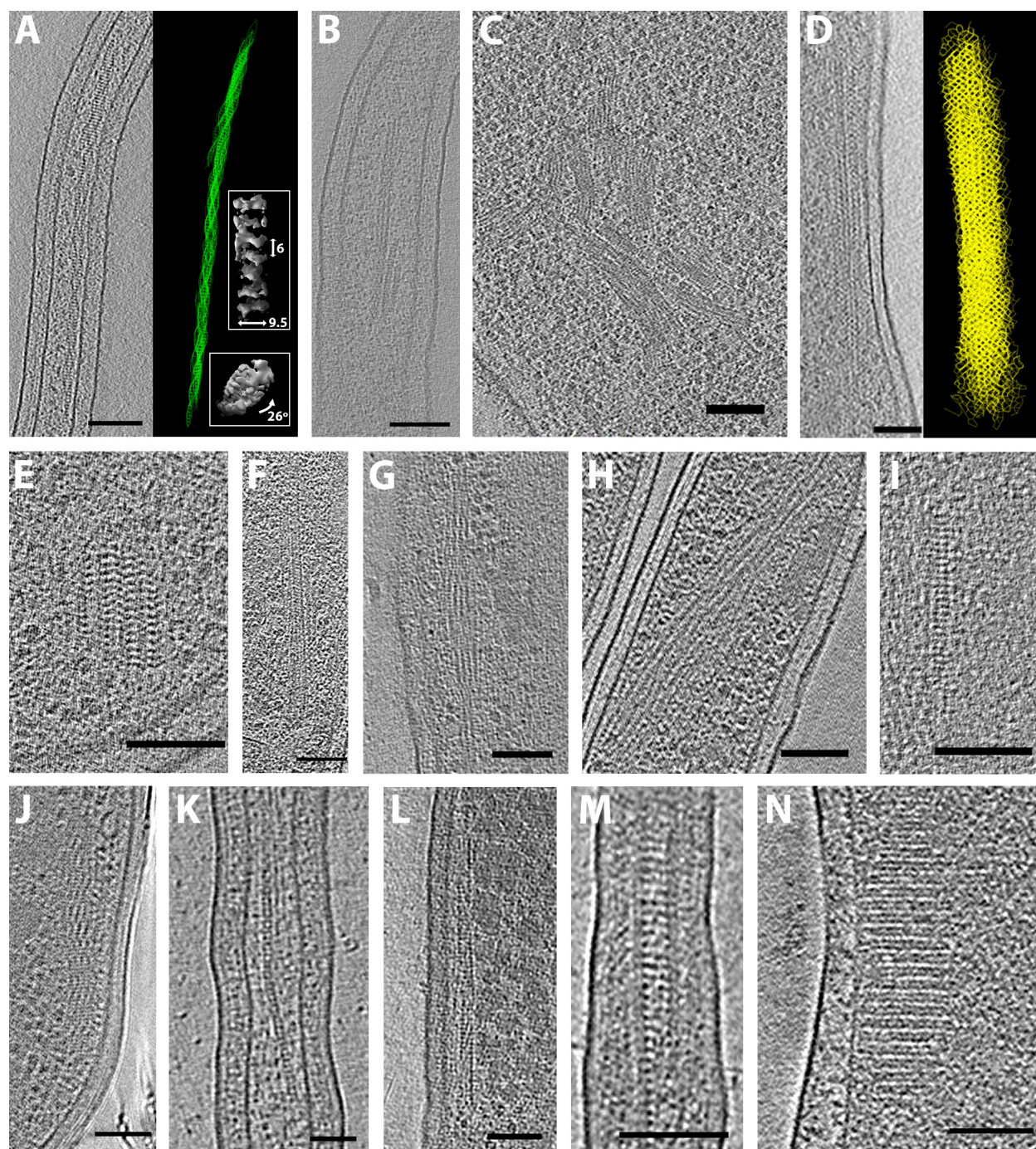


Figure 6

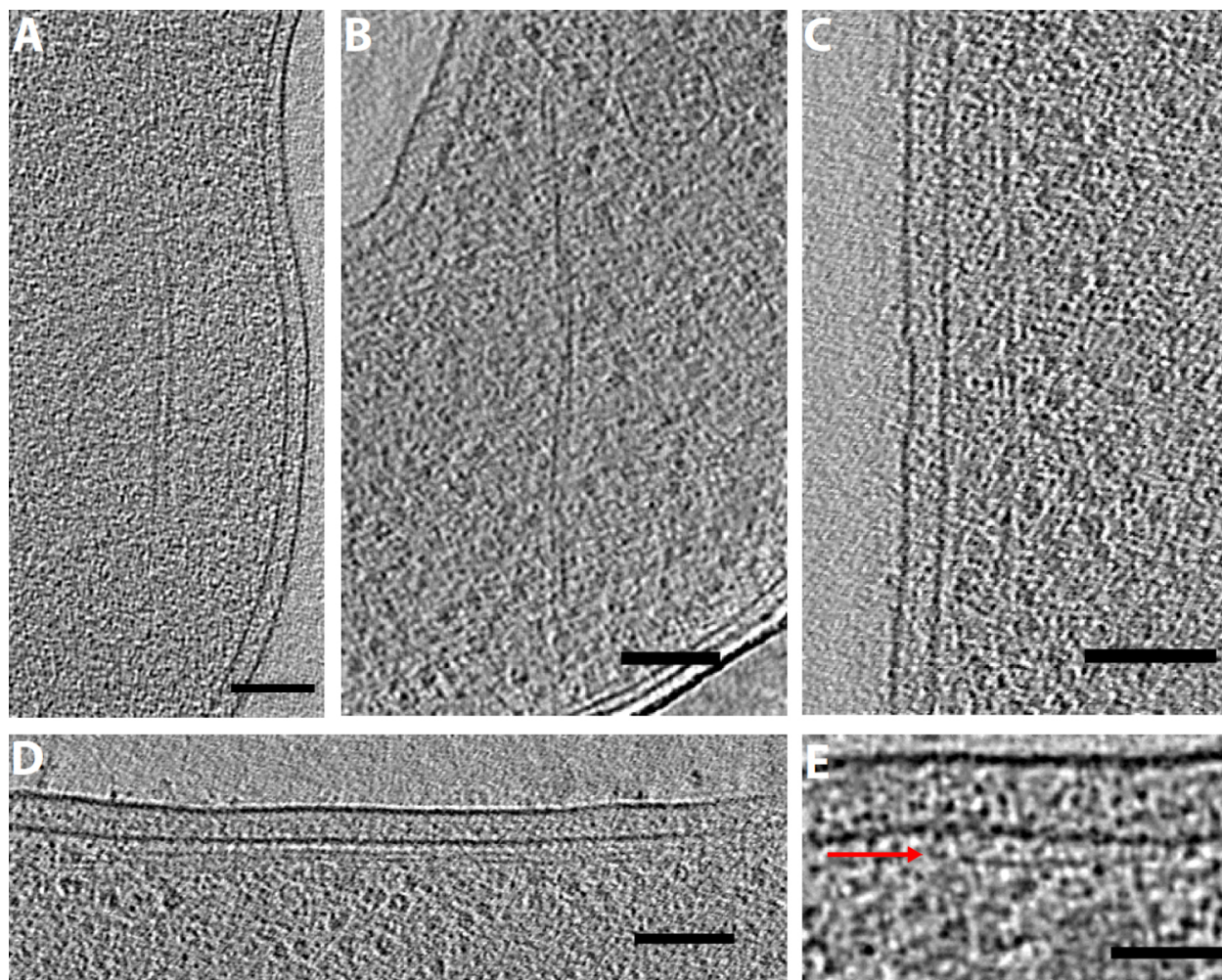


Figure 7

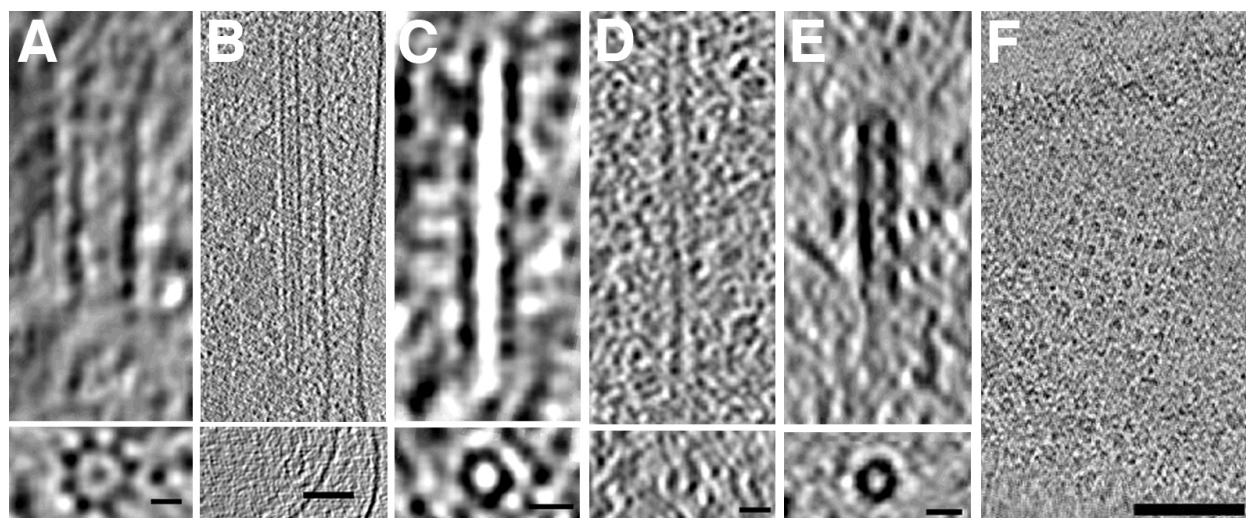


Figure 8

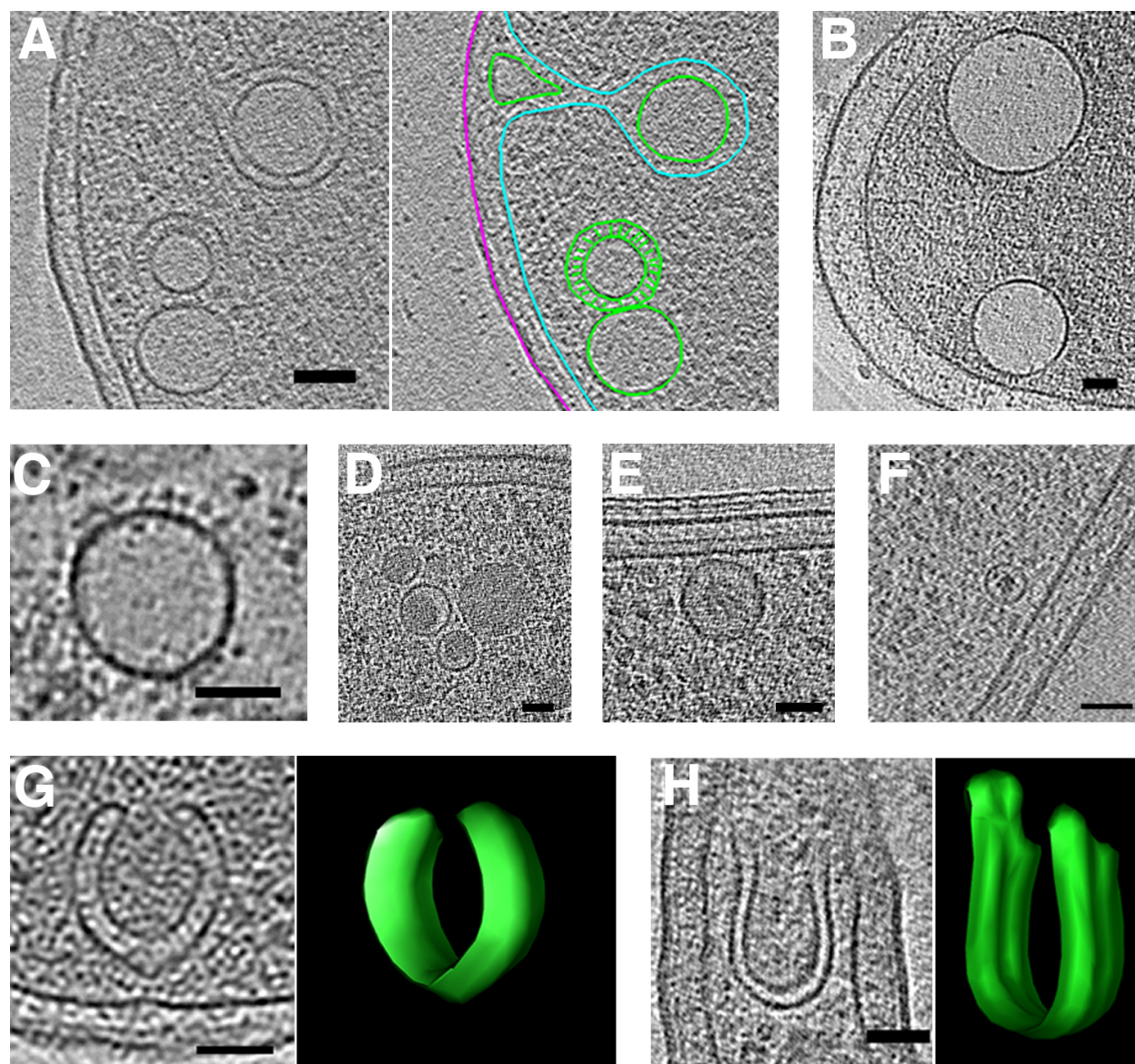


Figure 9

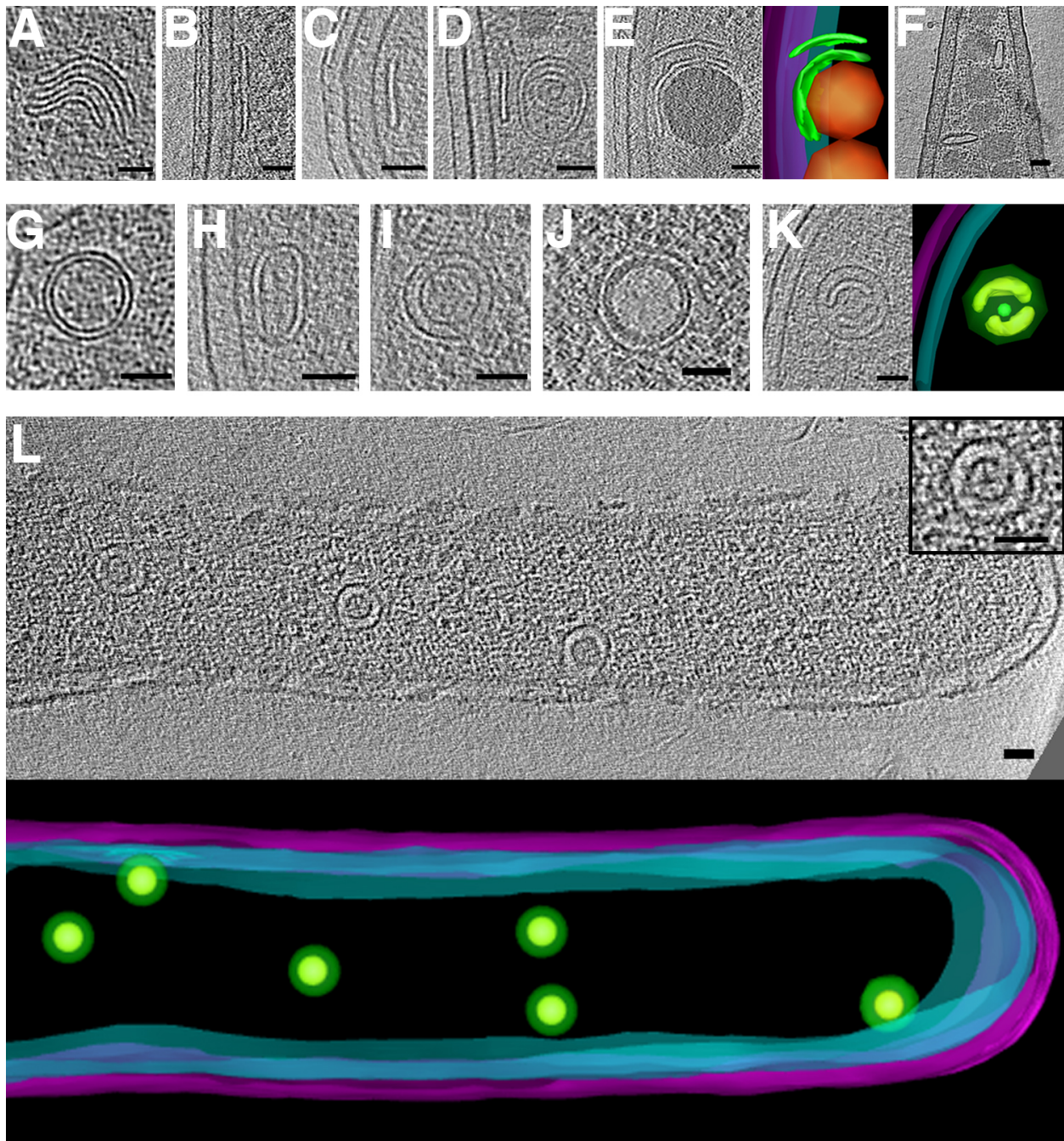


Figure 10

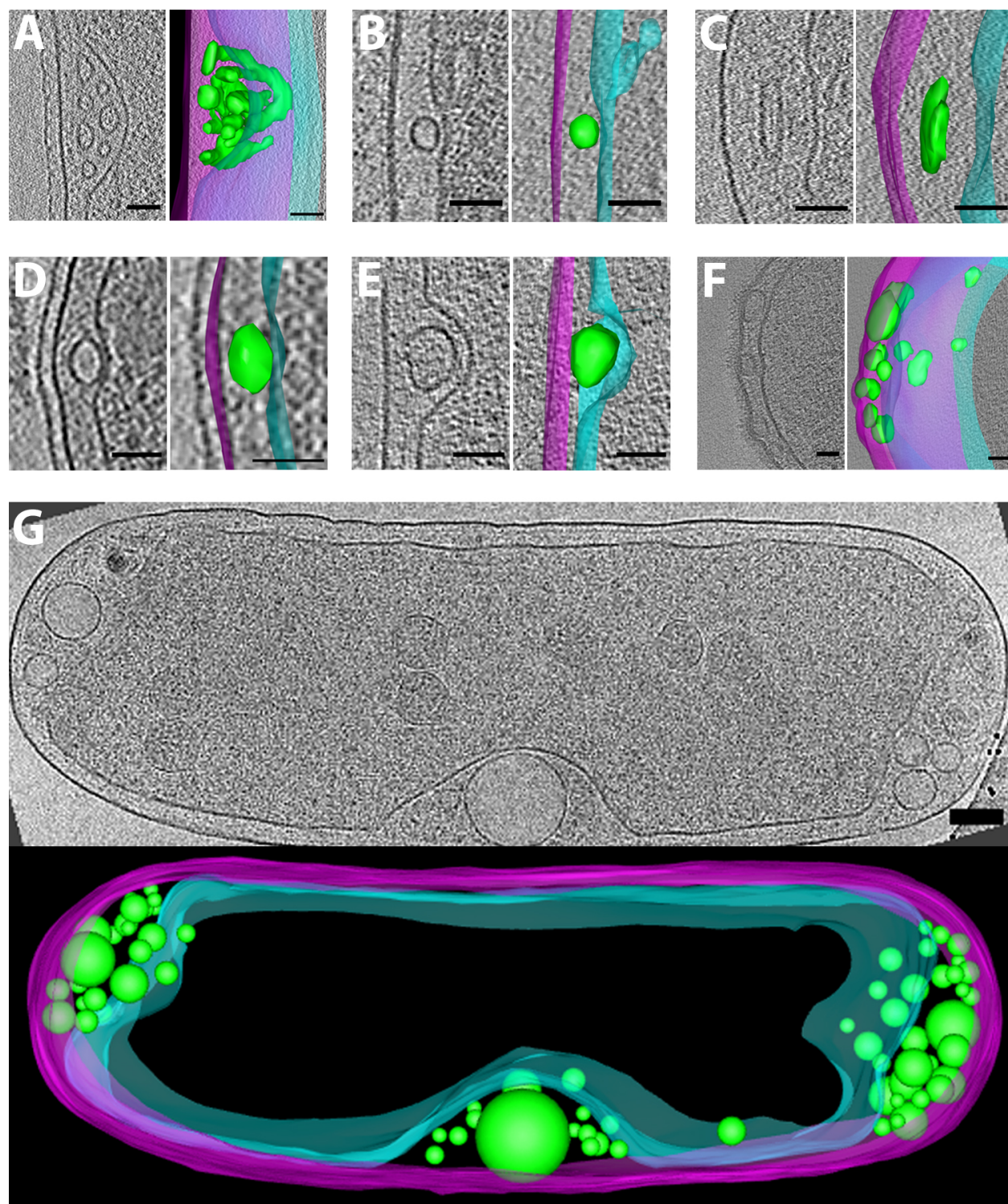


Figure 11